Control of diamond film microstructure by Ar additions to CH$_4$/H$_2$ microwave plasmas

D. Zhou,[a] D. M. Gruen,[b] L. C. Qin, T. G. McCauley, and A. R. Krauss
Materials Science and Chemistry Divisions, Argonne National Laboratory, Argonne Illinois 60439

The transition from microcrystalline to nanocrystalline diamond films grown from Ar/H$_2$/CH$_4$ microwave plasmas has been investigated. Both the cross-section and plan-view micrographs of scanning electron microscopy reveal that the surface morphology, the grain size, and the growth mechanism of the diamond films depend strongly on the ratio of Ar to H$_2$ in the reactant gases. Microcrystalline grain size and columnar growth have been observed from films produced from Ar/H$_2$/CH$_4$ microwave discharges with low concentrations of Ar in the reactant gases. By contrast, the films grown from Ar/H$_2$/CH$_4$ microwave plasmas with a high concentration of Ar in the reactant gases consist of phase pure nanocrystalline diamond, which has been characterized by transmission electron microscopy, selected area electron diffraction, and electron energy loss spectroscopy. X-ray diffraction and Raman spectroscopy reveal that the width of the diffraction peaks and the Raman bands of the as-grown films depends on the ratio of Ar to H$_2$ in the plasmas and are attributed to the transition from micron to nanometer size crystallites. It has been demonstrated that the microstructure of diamond films deposited from Ar/H$_2$/CH$_4$ plasmas can be controlled by varying the ratio of Ar to H$_2$ in the reactant gas. The transition becomes pronounced at an Ar/H$_2$ volume ratio of 4, and the microcrystalline diamond films are totally transformed to nanocrystalline diamond at an Ar/H$_2$ volume ratio of 9. The transition in microstructure is presumably due to a change in growth mechanism from CH$_3\cdot$ in high hydrogen content to C$_2$ as a growth species in low hydrogen content plasmas. [S0021-8979(98)07316-2]

I. INTRODUCTION

Polycrystalline diamond films whose microstructure typically consist of crystallites with sizes on the order of microns have been synthesized by a variety of chemical vapor deposition (CVD) techniques from methane–hydrogen mixtures.[1–3] Atomic hydrogen has been recognized to play a crucial role in the growth of phase-pure microcrystalline diamond films by the CVD techniques, typically using hydrocarbons as the carbon source.[4–6] Atomic hydrogen is thought to play a number of roles including abstraction reactions, termination of carbon dangling bonds, and regasification of nondiamond materials at the growth surface.[7–9] Reducing the concentration of hydrogen while continually increasing the hydrocarbon content of the plasma normally causes the growth of nondiamond phases and eventually the complete absence of the diamond phase.[10,11] The grain size, surface morphology, and surface roughness of the polycrystalline diamond films prepared from hydrogen-rich plasmas depend strongly on the film thickness. Generally, the thicker the film, the larger the grain size and the rougher the surface of the film. This behavior is generally ascribed to growth competition between differently oriented grains, with grain growth in turn being strongly correlated with surface roughness as discussed in more detail below. Many applications of CVD diamond films, however, require smooth surfaces, which are not readily prepared from hydrogen-rich plasmas. The ability to control the microstructure and the surface morphology of diamond films, therefore, could be important for tailoring this unique material to a variety of applications.

It has been found that a number of properties, including surface morphology and crystal orientation of microcrystalline diamond films, depend on a variety of factors such as the nucleation process and film deposition conditions.[12–14] Microcrystalline diamond films grown from randomly oriented nuclei exhibit columnar growth, which is caused by an ''evolutionary selection'' of crystallites.[15] Because crystals with a direction of fastest growth more or less perpendicular to the substrate grow at the expense of less favorably oriented ones, only a few crystallites survive, and a highly textured film consisting of larger, columnar crystallites is formed after a longer period of growth. The grain size therefore increases with the thickness of the films, and usually the larger the grains the rougher the surface of the films. Therefore, if it were possible to reduce the grain size in a controlled way, smoother surfaces should result.

In order to understand and control surface morphology and crystal orientation, both the nucleation and deposition processes have been investigated extensively.[16–20] It has been found that diamond films can be grown with a preferred orientation, such as ⟨111⟩ or ⟨110⟩, by precisely controlling the prenucleation treatments and the deposition process parameters. Moreover, it has been recognized that nitrogen and oxygen additions in the plasmas have a strong effect on the growth morphology of diamond films.[21–24] In other studies,

a)Present address: Department of Mechanical, Materials, and Aerospace Engineering, Advanced Materials Processing and Analysis Center, University of Central Florida, Orlando, Florida 32816; electronic mail: dzhou@pegasus.cc.ucf.edu

b)Author to whom correspondence should be addressed; electronic mail: gruen@anichm.chm.anl.gov

to increase the electron density of the plasma and to modify diamond film morphology, argon has been added to plasmas.[25] Argon has also been used in place of hydrogen in a carbon–oxygen–argon system, but oxygen was found to be a critical parameter for the phase purity of the deposited diamond films.[26] Furthermore, in a microwave methane–hydrogen plasma, noble gases were found to have a profound effect on plasma chemistry, including additional ionization and dissociation. Upon adding a noble gas such as Ar, the emission intensity of various species changes and the growth rate of diamond is enhanced.[27] However, the effect of Ar addition to the microwave discharges, and thus the microstructures of the deposited films at concentrations higher than about 30 vol % have not been studied in detail.

Recently, it has been reported that nanocrystalline diamond films can be grown from an Ar–C_{60} microwave plasma without adding molecular hydrogen to the reactant gas.[28] In that experiment, fullerenes such as C_{60} and C_{70} have been used as the carbon source for nanocrystalline diamond growth. Fragmentation of the fullerenes in the plasma results in strong Swan band emission due to C_2 radicals. The C_2 dimer appears to be the growth species for nanocrystalline diamond.[29,30] Furthermore, nanocrystalline diamond films have also been synthesized from Ar/CH_4 microwave discharges, without the addition of molecular hydrogen.[31] Atomic force microscopy (AFM) shows that the surface roughness is in the range of 20–50 nm, independent of the film thickness, thus suggesting that grain size remains in the nanometer range. Some of the unique properties of such nanocrystalline films have been characterized, including their tribiological[32] and electron field emission properties.[33]

In the present article, we report on a method that allows one to control the microstructure of diamond films grown from Ar/H_2/CH_4 plasmas. The factors leading to a transition from microcrystalline to nanocrystalline diamond have been investigated. The as-grown films produced from Ar/H_2/CH_4 plasmas with different ratios of Ar to H_2 have been characterized by scanning electron microscopy (SEM), micro-Raman spectroscopy, transmission electron microscopy (TEM), x-ray diffraction (XRD), and AFM.

II. EXPERIMENT

A microwave plasma enhanced CVD system (ASTeX PDS-17) has been employed for the diamond film preparations. Mixtures of CH_4, Ar, and H_2 have been used as the reactant gases for the microwave discharges. The flow rate of CH_4 was kept constant at 1 sccm, while the flow rate of Ar was varied from 0 to 99 sccm and supplemented by H_2 so as to maintain a 100 sccm total flow rate. *n*-type single crystal silicon wafers with an ⟨100⟩ orientation were used as the substrates, and mechanical polishing with fine diamond powder (0.1 μm) was employed to provide nucleation sites for the diamond film growth. During the deposition process, the substrate temperature, which was controlled by a separate heater, was maintained at 800 °C, while total ambient pressure and input power were kept at 100 Torr and 1200 W, respectively. The reactant gases used for each film deposition are listed in Table I. To investigate the effect of the concen-

TABLE I. Summary of the reactant gases used for diamond film depositions from microwave discharges.

Sample No.	Reactant gas (vol %)		
	Argon	Hydrogen	Methane
I	2	97	1
II	20	79	1
III	40	59	1
IV	60	39	1
V	80	19	1
VI	90	9	1
VII	97	2	1
VIII	99	0	1

tration of the C_2 dimer on the growth rate at a given Ar/H_2 ratio, the total pressure of the reactant gas (CH_4/Ar) was varied from 40 to 150 Torr.

In order to obtain some information on plasma species during the deposition process, optical emission was measured using a spectrometer equipped with a 1200 grooves/mm grating and a water-cooled photomultiplier tube (Interactive Technology). The concentration of C_2 dimers could be determined from the emission spectra because it was found in earlier work that emission is linearly correlated with quantitative absorption measurements.[34] Emission from the plasma was collected with a quartz optical fiber viewing a region 1–2 cm above the substrate. The monochromater was stepped in 2.0 Å increments with a dwell time of 100 ms from 3000 to 7000 Å. The emission intensity of C_2 was measured from the C_2 Swan system at 5165 Å. The growth rates of diamond thin films deposited from the Ar/H_2/CH_4 plasmas were determined by monitoring modulations of the surface reflectivity versus deposition time with a He–Ne laser (6328 Å) reflectance interferometer during the deposition process.[35] One peak-to-peak modulation represents 130 nm, and depositions were carried out until film thicknesses of about 5 μm were obtained.

The as-grown films were then investigated using a JEOL 840A SEM with a tungsten filament operating at 10 kV accelerating voltage and a probe current of 3×10^{-11} A. Both plan-view and cross-section SEM images were obtained to examine the surface and growth morphologies as a function of added Ar. A high-resolution JEOL 4000EX TEM operated at 400 kV accelerating voltage and a Philips CM30 analytical TEM equipped with a Gatan electron energy loss spectroscopy (EELS) spectrometer were employed for detailed microstructural characterization of selected films. The plan-view TEM samples were prepared by the conventional methods, i.e., mechanical cutting, shaping, dimpling, and ion milling. In order to confirm the crystalline structure of the films, x-ray diffraction was conducted by using a Philips x-ray spectrometer with a copper K_α target. The starting and ending angles (2θ) for the x-ray diffraction are 20° and 120°, respectively. A Renishaw Raman Microscope (System 2000), which can capture both Raman spectra and images, was used for further characterization of the as-grown films. The light source for illuminating the sample is provided by a He–Ne laser (6328 Å). Raman spectra and images can be obtained via a grating or filter system. The Raman scattering produced by a sample was measured by a charge-coupled
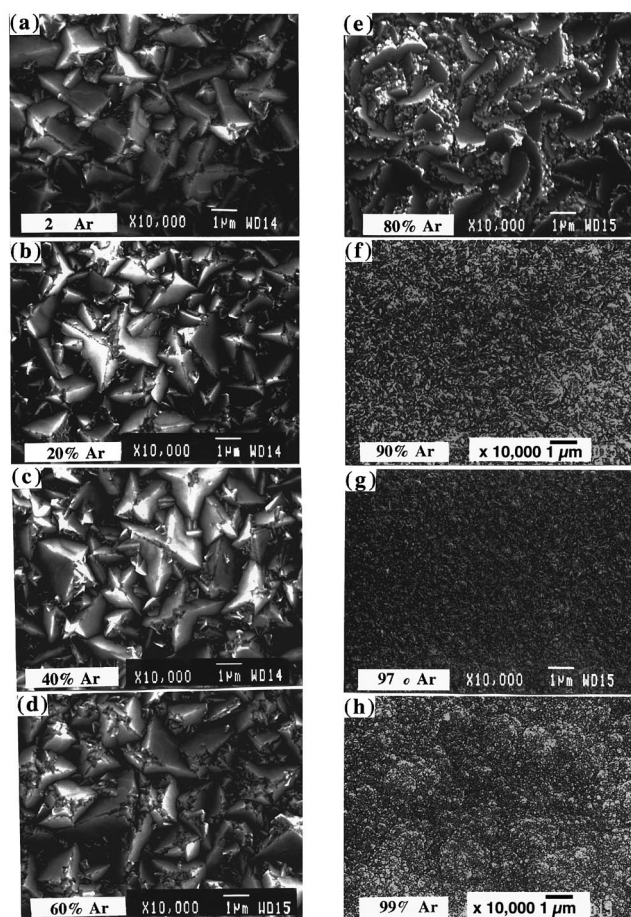
FIG. 1. The plan-view SEM images of the as-grown films prepared from microwave plasmas with different mixtures of Ar, H_2, and CH_4 as the reactant gases (listed in Table I) showing the transition of microcrystalline to nanocrystalline diamond films: (a) film I; (b) film II; (c) film III, (d) film IV; (e) film V; (f) film VI; (g) film VII and (h) film VIII.

device (CCD) camera. To obtain the planography and the surface roughness of the as-grown films, a Burleigh ARIS-3300 personal AFM with image resolution of x-y axes <30 Å and z axis <3 Å was used. The true image software manages the secondary signals sent to the electronic controller and displays the resulting images in close to real time.

III. RESULTS AND DISCUSSIONS

The as-grown films were first examined by SEM in order to obtain the surface and growth morphologies as a function of added Ar. The plan-view SEM images shown in Fig. 1 demonstrate a dramatic change in the surface morphology of the films when adding Ar gas to the H_2/CH_4 microwave plasma. Figure 1(a) shows the surface morphology of film I, displaying a well-facetted microcrystalline diamond surface with grain sizes ranging from 0.5 to 2.0 μm. The surface is very rough and consists of a combination of {111} and {110} facets. This SEM image suggests that the crystallite morphology of film I is independent of crystal orientation and that secondary nucleation rates must be very low. A plan-view SEM image of film II [see Fig. 1(b)] shows that {111} planes are still the preferred growth planes, but small diamond particles start to form on the surface of bigger dia-

mond grains during the deposition process, suggesting that secondary nucleation or renucleation occurs when 20% of Ar gas has been added to the microwave plasma. The number density of the small crystals increases significantly at the level of 40 to 60 vol % Ar [see Figs. 1(c) and 1(d) for films III and IV]. Note that these SEM images also show that most of the small diamond crystals nucleate and grow at the edges (twin boundaries) of larger diamond crystals. At 80 vol % Ar, the edges or the twins of the large-size diamond crystals begin to disappear, and well-facetted $\langle 111 \rangle$ as well as $\langle 110 \rangle$ diamond crystallites of micron size no longer exist, while small diamond crystals mixed with large diamond flakes are found in the plan-view SEM image [see Fig. 1(e) for film V]. When 90 vol % Ar is added to the $Ar/H_2/CH_4$ plasma, the crystal sizes are greatly reduced to the nanometer scale, and the surface structure of the diamond film [see Fig. 1(f) for film VI] changes from microcrystalline to nanocrystalline. At this point, facetted micron-size diamond has disappeared, and nanocrystalline diamond begins to predominate. Figures. 1(g) and 1(h) show the plan-view images of films VII and VIII, respectively, revealing that the crystal sizes of the nanocrystalline diamond can be further reduced when the plasma consists of 97% Ar [see Fig. 1(g)] or 99% Ar [see Fig. 1(h)]. In the latter case, the film was grown in the absence of added hydrogen.

This series of SEM micrographs demonstrates the transition of the microstructure of the films from microcrystalline to nanocrystalline diamond. In order to obtain information on the development of the growth morphology, films I, V, VI, and VII were selected for further investigation by cross-section SEM. Figure 2(a) shows the cross-section SEM image of film I with a columnar growth structure, which is typical of the growth morphology from H_2/CH_4 plasmas and reflects the van der Drift growth mechanism.[15] This columnar growth phenomenon suggests that atomic hydrogen plays an important role in suppressing secondary nucleation by regasifying small or nondiamond phase nuclei. Thus, only a few larger diamond crystals of micron size survive after a longer period of growth. The greater the Ar content of the microwave plasma, the greater the fraction of small diamond crystals. Figure 2(b) shows the cross-section SEM image of the as-grown diamond film V, displaying that the film still has columnar growth, but the columns are much narrower than those in film I. As the Ar volume fraction increases to 90 or 97 vol %, the columnar structure totally disappears from the cross-section SEM images of films VII and VIII [see Figs. 2(c) and 2(d)]. Instead, the cross-sectional views show smooth fracture surfaces, which suggests that the nanocrystalline diamond does not grow from the initial nuclei at the substrate–film interface, but is the result of very high renucleation rates. The mechanism of secondary nucleation with C_2 as the growth species is currently an active topic of investigation in our laboratory. Suffice it to say that the cross-section SEM images clearly show columnar growth, which gives way to highly dense continuous films with no distinctive growth morphology. The lack of morphological features is probably due to the fact that the crystallites are too small to be resolved in the SEM.
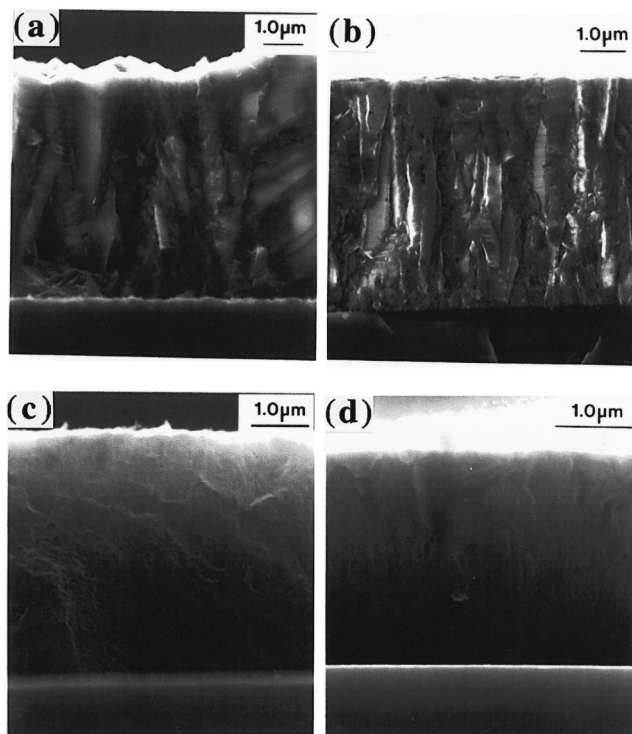
FIG. 2. The cross-section SEM images of the as-grown films prepared from microwave plasmas with different mixtures of Ar, H$_2$, and CH$_4$ as the reactant gases showing different growth phenomena of microcrystalline and nanocrystalline diamond films: (a) film I; (b) film V; (c) film VI; and (d) film VII.

X-ray powder diffraction has been used to characterize the crystalline structures of the films. Figure 3 shows the x-ray diffraction of films I, II, IV, V, and VI. The diffraction peaks can be indexed according to the cubic diamond structure, which means that all the films produced from either hydrogen-rich or argon-domain microwave plasmas consist of diamond crystals. The diffraction spectra show that with
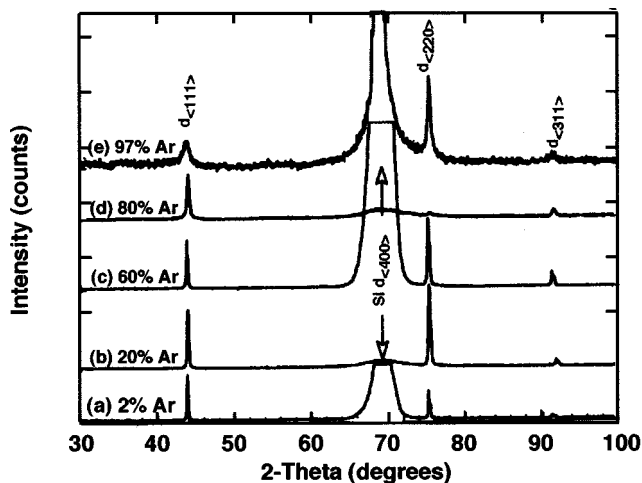
FIG. 3. The x-ray diffraction patterns of the as-grown films deposited from microwave plasmas with different mixtures of Ar, H$_2$, and CH$_4$ as the reactant gases showing that the films consist of crystalline diamond. The diffraction peaks broaden with increasing concentration of Ar due to decreasing grain size: (a) film I; (b) film II; (c) film IV; (d) film V; and (e) film VII.
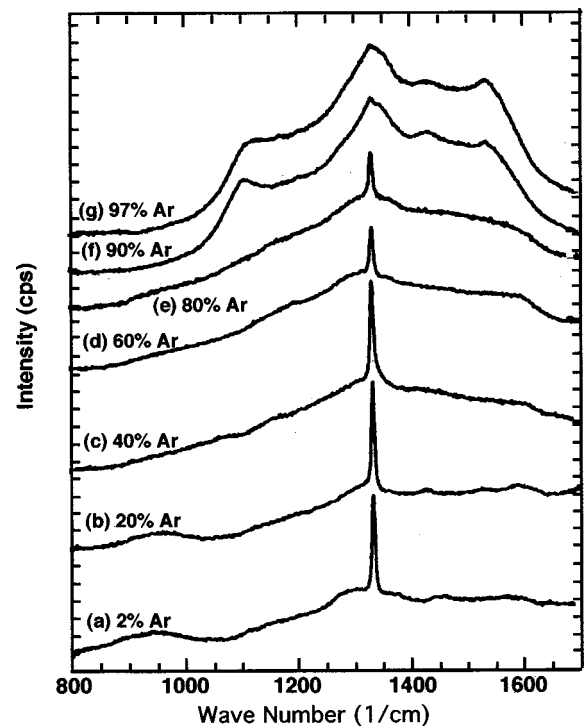

FIG. 4. Raman spectra of the as-grown films deposited from Ar/H$_2$/CH$_4$ microwave plasmas with different reactant gases show that Raman scattering is strongly influenced by grain size: (a) film I; (b) film II; (c) film III; (d) film IV; (e) film V; (f) film VI; and (g) film VII.

increasing volume percent of Ar, the widths at half height of the diffraction peaks increase significantly, which may be correlated with decreasing grain sizes. There is no evidence for the presence of graphitic or amorphous carbon in the x-ray diffraction patterns of both microdiamond and nanodiamond films. The ratio of the $\langle 111 \rangle$ to the $\langle 110 \rangle$ diffraction peak [see Figs. 3(a)–3(e)] increases greatly with increasing ratio of Ar to H$_2$, indicating that the diamond grains tend to orient with the {110} crystallographic planes parallel to the substrate surface when their sizes change to the nanometer scale. Note that the silicon diffraction peak from Si {400} planes derives from the substrate used for the film depositions.

X-ray and electron diffractions are sensitive to the presence of crystalline carbons such as diamond or graphite but less sensitive to amorphous carbon. In contrast, Raman scattering is about 50 times more sensitive to π-bonded amorphous carbon and graphite than to the phonon band of diamond, and hence it is frequently used to characterize CVD diamond films. Figure 4 shows the plots of Raman spectra of the as-grown films produced from Ar/H$_2$/CH$_4$ microwave plasmas with different ratios of Ar/H$_2$ in the reactant gases, revealing the transition from microcrystalline to nanocrystalline diamond films. For film I grown from the Ar/H$_2$/CH$_4$ microwave plasma with 2 vol % Ar addition, the spectrum shows a sharp Raman band at 1332 cm^{-1}, characteristic of diamond. Little Raman scattering in the range 1450–1490 cm^{-1} (graphite band) caused by carbon sp^2 bonded carbon is observed. When adding argon to the reactant gas up to 40 vol %, the Raman spectra of films II and III still demonstrate the presence primarily of microcrystalline
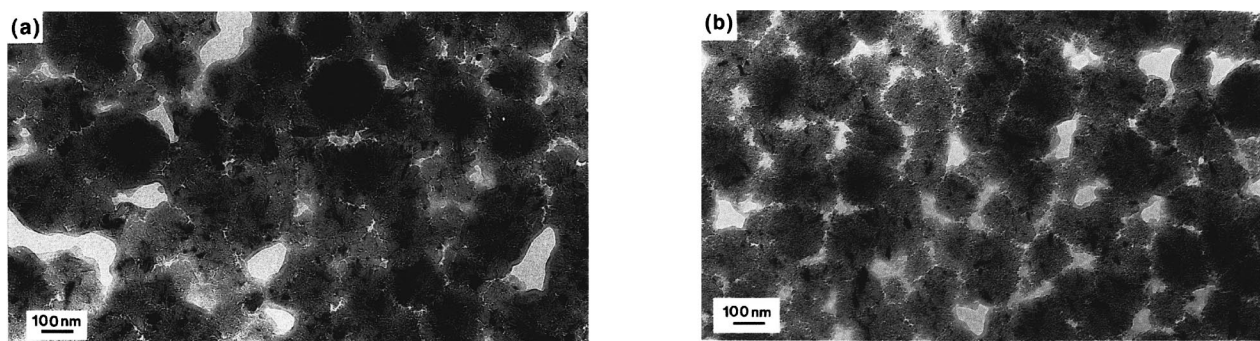
FIG. 5. Plan-view TEM images of nanocrystalline diamond films produced from $Ar/H_2/CH_4$ microwave discharges showing the effect of the concentration of Ar or H_2 on the the grain size: (a) film VI with grain sizes ranging from 30 to 50 nm; (b) film VII with grain sizes in the range of 10–30 nm.

diamond, although the spectra are slightly broadened. Further increasing the concentration of Ar in the plasmas results in the shrinking of the diamond band and increasing its width at full width half maximum (FWHM) (see spectra for the films IV and V). When more than 90 vol % of Ar is added to the plasma, Raman spectra of the films VI and VII typically show nanocrystalline features. The diamond band at 1332 cm^{-1} is significantly broadened, and Raman scattering intensity in the 1400–1600 cm^{-1} region is pronounced. It has been shown that broadening of the diamond band is
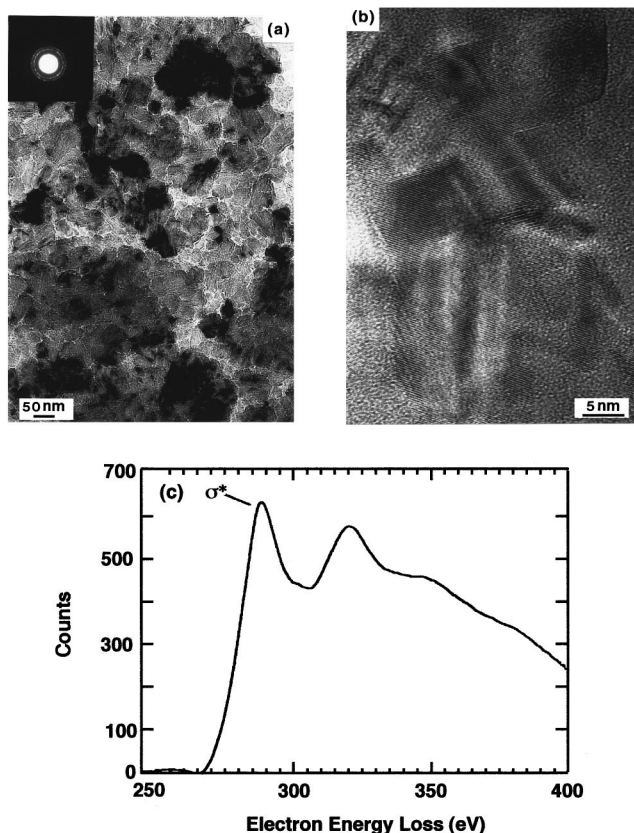

FIG. 6. (a) A plan-view TEM image of diamond film (VIII) produced from 1% CH_4+99% Ar composition, demonstrating that the film consists of very small grains ranging from 3 to 25 nm; (b) a high-resolution lattice fringe TEM image of the film, (c) electron energy loss spectrum of the film from an area over 10 μm in diameter showing the σ^* edge. The inset images show the selected area electron diffraction patterns of the film.
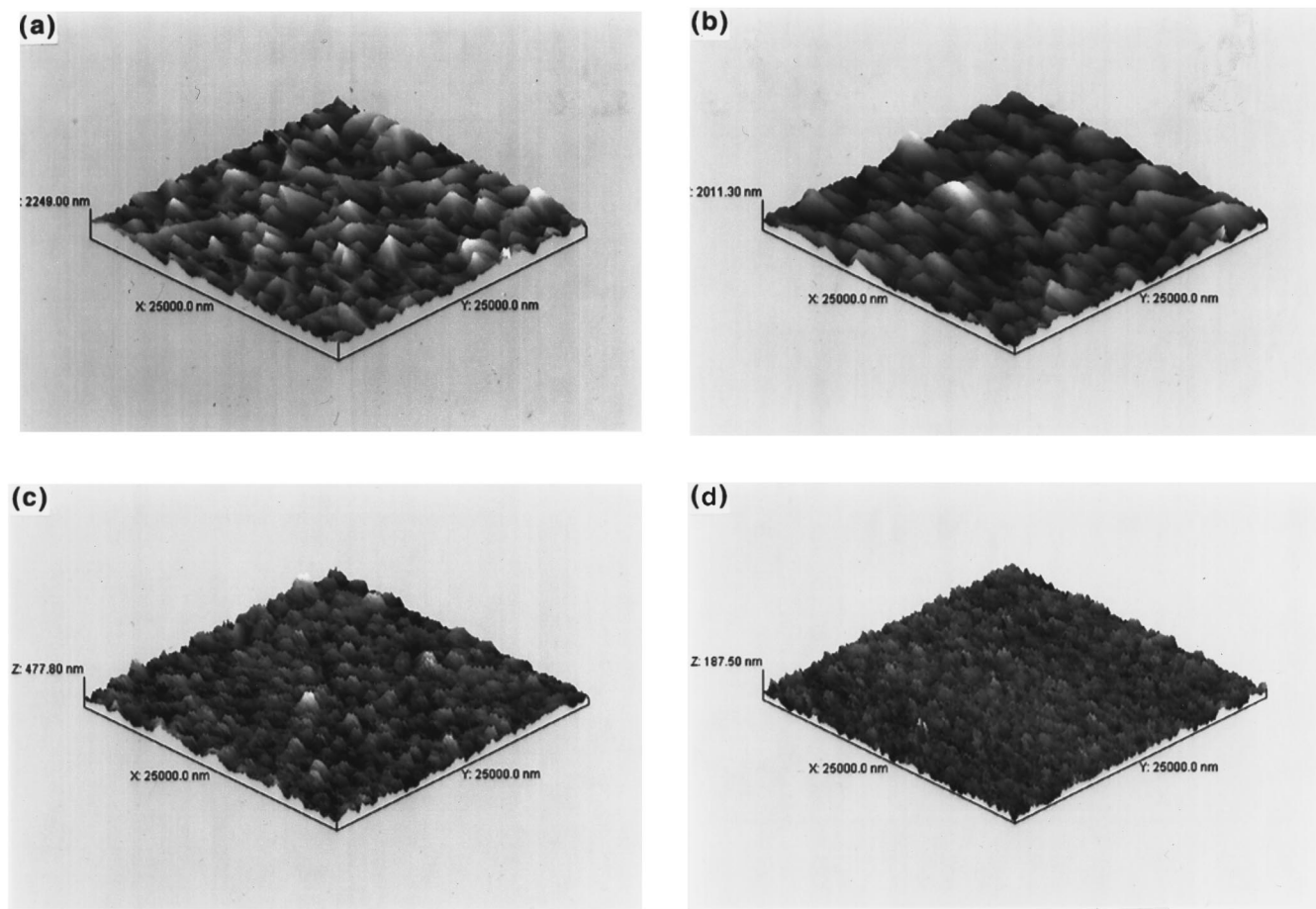
caused by decreasing the grain size to the nanometer scale, and the development of the "graphite" band is due to increasing π-bonded carbon at the grain boundaries in the nanocrystalline films.[36,37] The grain boundaries consist of carbon atoms with a sp^2 electron configuration. Note that besides the diamond and graphite bands, the spectra also have an extra Raman shift around 1150 cm^{-1}, which may be caused by nanocrystalline diamond.[38] Therefore, in addition to SEM images and x-ray diffraction, Raman spectra of the as-grown films further confirm the transition of microdiamond to nanodiamond prepared from microwave plasmas as argon is added to CH_4H_2 mixtures.

A powerful way to study the effect of added Ar on grain size is with TEM. Examples of the application of this technique to the present study are given below. Figure 5(a) shows a plan-view TEM image of film VI (90 vol % Ar) with grain sizes ranging from 30 to 50 nm. However, film VII (97 vol % Ar) has grain sizes in the range of 10–30 nm [see Fig. 5(b)]. Thus, the grain size of the nanocrystalline diamond decreases strongly in the range 90–97 vol % Ar. Further characterization of the nanocrystalline film VIII (99 vol % Ar) has been conducted by high-resolution TEM and EELS observations. Figure 6(a) shows a plan-view TEM image of film VIII with grain sizes ranging from 3 to 20 nm. The inset image is a selected area (over 10 μm in diameter) electron diffraction pattern, which can be fully indexed on the diamond structure. A high-resolution TEM image shown in Fig. 6(b) demonstrates that individual diamond grains are single crystals with sizes in the 10–20 nm range. The image of lattice fringes has a spacing of 0.205 nm, which is the interplanar distance between diamond {111} planes. Note that the lattice image of diamond can only be observed on {111} planes and only when they are properly oriented, since the TEM resolution is about 1.8 Å. EELS has been employed as a diagnostic for amorphous or disordered carbon with sp^2 bonding. It is known that the different carbon phases have very distinct K-shell absorption edge structures. Diamond has a single EELS feature with an onset at 289 eV due to its σ^* electronic state, while graphitic or amorphous carbon has an additional EELS edge starting at 284 eV, owing to its lower lying antibonding π^* state.[39] Figure 6(c) shows an EELS spectrum of the nanocrystalline diamond film produced from an Ar/CH_4 plasma acquired over an area ~10

FIG. 7. Three-dimensional AFM images of the as-grown diamond films deposited from Ar/H_2/CH_4 microwave plasmas with different reactant gases showing the effects of increasing the ratio of Ar to H_2 in the reactant gas on the surface morphology and surface roughness of the as-grown films: (a) film I; (b) film IV; (c) film VI; (d) film VII.

μm in diameter, displaying only an EELS edge at 289 eV, characteristic of diamond. No energy loss feature at 284 eV has been observed, demonstrating the absence of an amorphous or graphitic phase in the film. These TEM analyses (plan-view and high-resolution TEM images as well as the EELS spectrum) confirm that film VIII prepared from an Ar/CH_4 microwave discharge without any H_2 addition is composed of nanocrystalline diamond.

To obtain information on planography and surface roughness, AFM has been employed. Note that all of the films for the AFM analyses have similar thicknesses of about 5 μm. Figure 7(a) shows a three-dimensional AFM image of film I (2 vol % Ar) with an rms (root mean square) surface roughness of about 425.43 nm. Addition of Ar up to 60 vol % decreases the rms roughness of film III to 262.76 nm, because this film consists of a significant amount of small diamond particles [see Fig. 7(b)]. When Ar in the plasma is further increased, the surface roughness of film VI (90 vol % Ar) is greatly reduced to 54.19 nm [see Fig. 7(c)]. With a reactant gas mixture of 97 vol % Ar, 2 vol % H_2, and 1 vol % CH_4, the AFM image shown in Fig. 7(d) reveals that the surface roughness of film VII is just 18.84 nm, a typical value for our nanocrystalline diamond films. Note that the rms roughness of film VII is about 25 times smaller than that of microcrystalline diamond film I. The detailed surface ana-

lytical data acquired by AFM characterization for films I, III, VI, and VII are listed in Table II, where Z-rms is the root mean square of the surface, Z-var is the average height of the surface, and Z-peak is the height difference between the highest and lowest points on the surface. A plot of the surface roughness of the films versus the concentration of Ar in the reactant gas is shown in Fig. 8. A plot of the data suggests an almost linear relationship between surface roughness of the films and volume % Ar. Since the ratio of Ar to H_2 in the reactant gas strongly affects the surface morphology and microstructure of the diamond films, this parameter can clearly be very useful in tailoring important properties of this material.

TABLE II. Summary of the surface morphologies of selected diamond films, measured by AFM. Z-rms is the root mean square of the surface; Z-var is the average height of the surface; Z-peak is the height difference between the highest and lowest points on the surface.

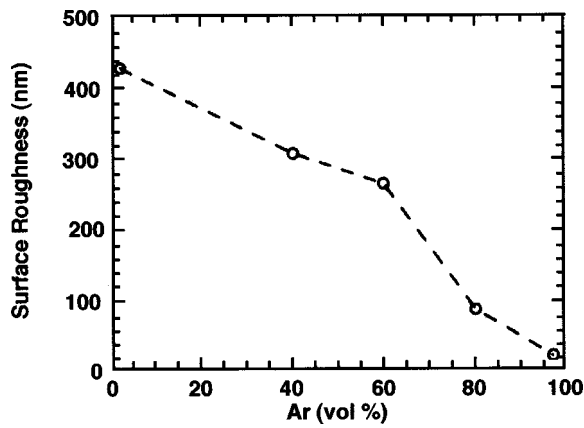| Sample No.	Z-avg (nm)	Z-rms (nm)	Z-var (nm)	Z-peak (nm)
I	1215.94	425.43	390.03	2249.02
IV	722.01	262.76	206.29	2011.31
VI	176.07	54.19	42.47	477.81
VII	58.38	18.84	14.84	187.51

FIG. 8. A plot of the surface roughness of the as-grown diamond films versus the concentration of Ar in the $Ar/H_2/CH_4$ microwave plasmas.

These profound changes in microstructure must reflect equally profound changes in the plasma chemistry. Optical emission spectroscopy has been employed to investigate the $Ar/H_2/CH_4$ plasmas in order to monitor C_2 dimer and atomic hydrogen concentrations in the microwave discharges. It has earlier been proposed that C_2 dimer is the growth species for nanocrystalline diamond.[28] The emission intensities of C_2 dimer from the discharges, which correlate linearly with the absolute C_2 concentration in $Ar/H_2/CH_4$ microwave plasmas,[34] are directly measured using the C_2 Swan system (5165 Å bands). Figure 9 shows the optical emission spectra of plasmas with different ratio of Ar to H_2. At 2% Ar the major optical emission peak is due to atomic hydrogen (H_α). Under these conditions, $CH_3\bullet$ is generally believed to be the important growth species, and its concentration has been
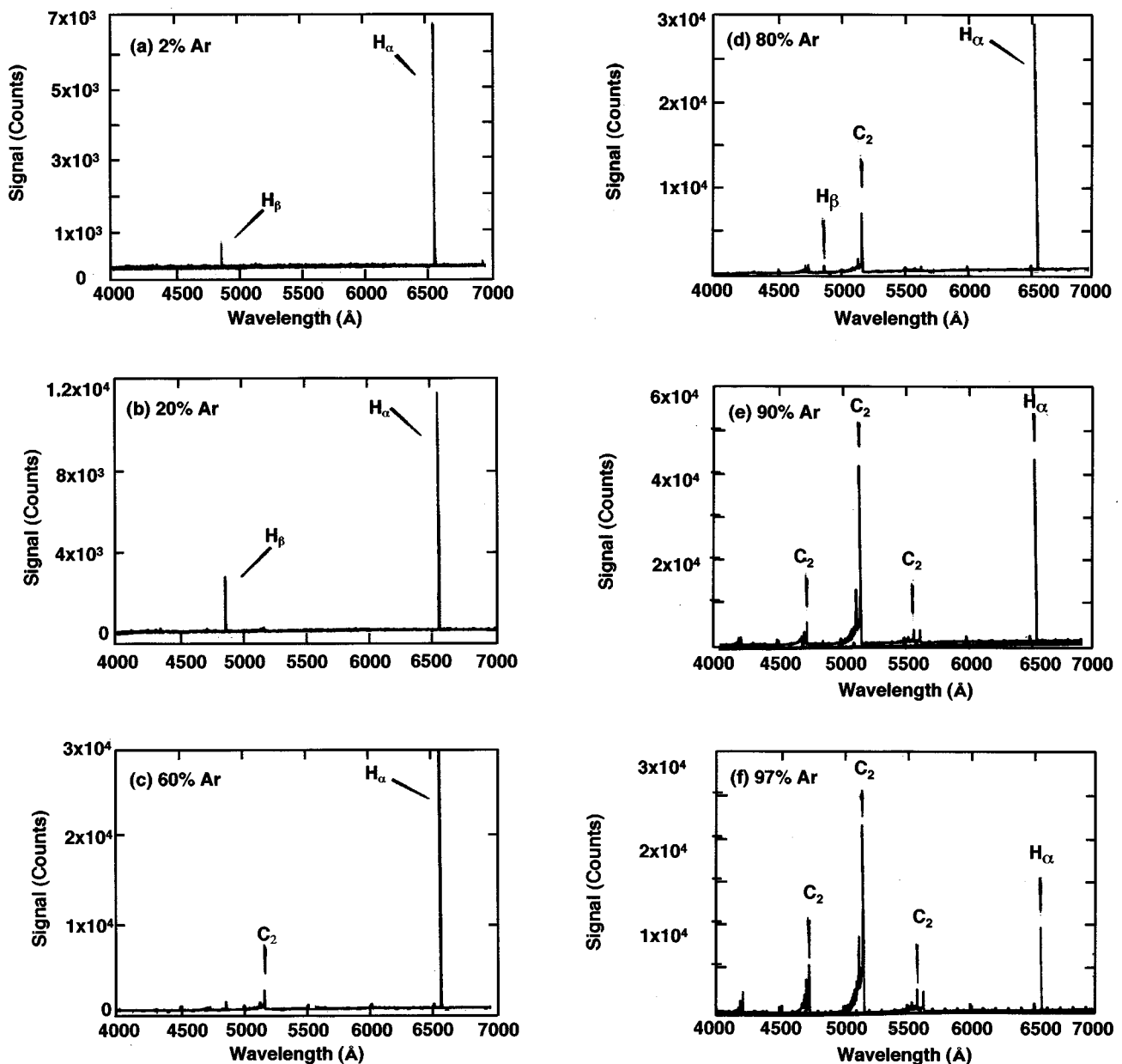

FIG. 9. The optical emission spectra of the $Ar/H_2/CH_4$ microwave plasmas with different mixtures of Ar, H_2, and CH_4 in the reactant gases: (a) 2% Ar+97% H_2+1% CH_4; (b) 20% Ar+69% H_2+1% CH_4; (c) 60% Ar+39% H_2+1% CH_4; (d) 80% AR+19% H_2+1% CH_4; (e) 90% Ar+9% H_2+1% CH_4; (f) 97% Ar+2% H_2+1% CH_4.
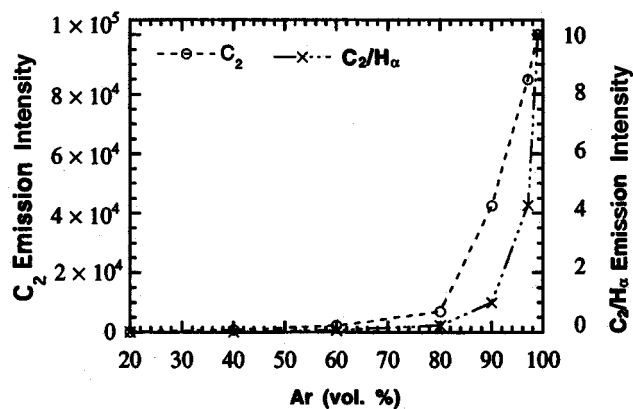
FIG. 10. Plots of the emission intensity of C_2 and the ratio of the emission intensities of C_2 to H_α vs the concentrations of Ar in the reactant gases.

FIG. 12. Plots of growth rates of nanocrystalline diamond films grown from Ar/CH_4 microwave plasmas and the emission intensities of C_2 vs reactant gas pressures for the discharges.

measured by others in absorption. Increasing the Ar concentration to 20 vol %, H_α emission is still the major feature [see Fig. 9(b)]. At 60 vol % Ar, we begin to observe emission from C_2 dimers in addition to H_α [see Fig. 9(c)]. Increasing the concentration of Ar increases the emission intensity of C_2 dimers [see Figs. 9(d)–9(f)] still further. The emission intensities of C_2 and the ratios of the emission intensities of C_2 to H_α versus vol % Ar are plotted in Fig. 10. Both are seen to increase by an order of magnitude in the range 80–97 vol % Ar. This has already been shown to be the region of most profound and rapid change in the microstructure of the diamond films.

Besides surface morphology, microstructure, and growth mechanism, the growth rate of diamond film has also been found to depend significantly on the ratio of Ar to H_2 in the reactant gas presumably because of effects on the microwave discharge chemistry. Figure 11 shows the growth rates of diamond films grown from 1% CH_4 in Ar–H_2 mixtures as a function of vol % Ar. The growth rates of the films were determined by monitoring modulations of the surface reflectivity versus deposition time with a He–Ne laser (6328 Å) reflectance interferometer. According to Fig. 11, the growth rate approximately doubles with Ar addition up to 60 vol % Ar and then decreases quite rapidly in the range of 80–97 vol % Ar. Although increasing Ar in the reactant gas from 80
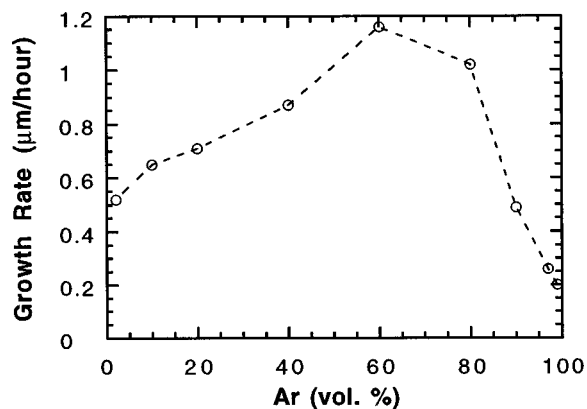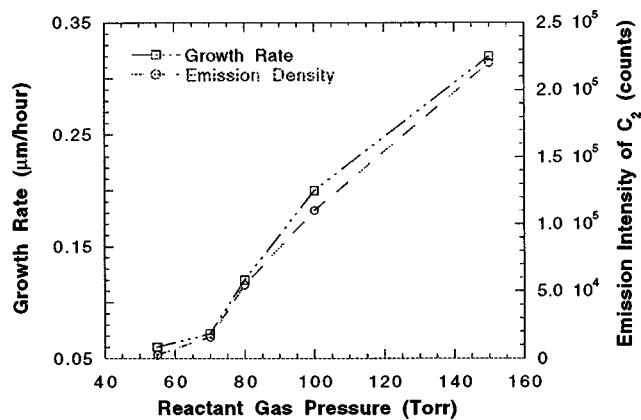
to 99 vol % significantly increases the concentration of C_2 dimer in the discharge (see Fig. 10), the growth rate in this region nonetheless decreases. Theoretical calculations have shown[30] that there is a pathway for the growth of diamond with C_2 as the growth species that involves hydrogen addition. This pathway has a lower energy of activation than the alternative pathway that does not involve the intervention of hydrogen, thus rationalizing the effect of hydrogen on the growth rate of nanocrystalline diamond in the range 80–99 vol % Ar. A great deal of further work needs to be done to reach a complete understanding of the effect of Ar addition on diamond film growth rate in the CH_4/H_2/Ar system.

In view of the above observations, it is important to investigate the effect of the C_2 concentration on the growth rate under the condition of constant hydrogen concentration. The reactant gas for this experiment is Ar/CH_4 without the addition of molecular hydrogen. The total pressure of the reactant gas was varied, but the ratio of Ar to CH_4 was fixed. Figure 12 shows plots of the growth rates of nanocrystalline diamond films and emission intensities of C_2 from the Ar/CH_4 plasmas versus reactant gas pressures ranging from 55 to 150 Torr. One finds that pressure strongly affects both the C_2 concentration and film growth rate. When the reactant gas pressure is below 40 Torr, no C_2 emission is detected, and no diamond film deposition is observed. Similarly, diamond film growth was not observed from Ar/CH_4 plasmas up to 15 Torr.[40] At 55 Torr, there is a very low emission intensity of C_2, accompanied by a correspondingly low growth rate of about 0.06 μm/h. As the reactant gas pressure increases, both the emission intensity of the C_2 dimers and the growth rate of the nanocrystalline films is increased significantly (see Fig. 12). The close relationship between the growth rate and the C_2 concentration shown in Fig. 12 suggests that the concentration of C_2 in the Ar/CH_4 plasma is the factor determining the film growth rate under conditions of low and constant H_2 concentration. Our observations demonstrate that the reactant gas pressure plays an important role in enhancing the intensity and therefore the concentration of C_2 in Ar/CH_4 plasma. That C_2 is the growth species for nanocrystalline diamond is confirmed by the functional relationship between the C_2 concentration and the growth rate.

FIG. 11. The growth rates of the diamond films from the Ar/H_2/CH_4 microwave discharges vs the concentration of Ar in the reactant gases.

J. Appl. Phys., Vol. 84, No. 4, 15 August 1998

Zhou *et al.*   1989

IV. CONCLUSIONS

The growth of diamond films from $Ar/H_2/CH_4$ microwave discharges has been studied systematically. We report a new way to control the surface morphology, grain size, and growth mechanism of diamond films by changing the ratio of Ar to H_2 in the reactant gases in a systematic way. Based on SEM plan-view images of the films, it has been demonstrated that a transition from microcrystalline to nanocrystalline diamond occurs in the range from 2 to 97 vol % Ar. Cross-section SEM shows that the microcrystalline diamond films grown from the microwave discharges have columnar growth, while the fracture surfaces of the nanocrystalline diamond films are very smooth, thus suggesting a different growth mechanism. This transition from microdiamond to nanodiamond with an increase of the Ar concentration in the reactant gas has been further confirmed by XRD and Raman spectroscopy. TEM and EELS characterization demonstrates the nanocrystalline nature of the films grown from $Ar/H_2/CH_4$ microwave plasmas with an Ar concentration in the range 80–97 vol %. The grain sizes of the nanodiamond range from 3 to 50 nm, depending on the ratio of Ar to H_2 in the reactant gas. The surface roughness of the films is strongly affected by the microstructure and the growth mechanism. AFM analysis shows that the surface roughness of the films with the same thicknesses changes from 425 nm for microdiamond to 18 nm for nanodiamond.

An optical emission study of the $Ar/H_2/CH_4$ microwave discharges shows that the ratio of Ar to H_2 in the reactant gas strongly affects the discharge chemistry. Increasing the concentration of Ar in the reactant gas significantly promotes the concentration of C_2 dimer in the discharge, which is important for nanocrystalline growth. By varying the reactant gas (CH_4/Ar) pressure from 40 to 150 Torr, a close relationship between the growth rate of the nanocrystalline diamond film and the concentration of C_2 dimer in the plasma has been observed, confirming that C_2 dimer is the growth species of the nanocrystalline diamond.

ACKNOWLEDGMENTS

[1] B. V. Spitsyn, L. L. BOuilov, and B. V. Derjagin, J. Cryst. Growth **52**, 219 (1981).

[2] M. Kamo, U. Sato, S. Matsumoto, and N. Setaka, J. Cryst. Growth **62**, 642 (1983).

[3] J. C. Angus and C. C. Hayman, Science **241**, 913 (1988).

[4] B. V. Deryagin, D. V. Fedoseev, N. D. Polyanskaya, and E. V. Statenkova, Sov. Phys. Crystallogr. **21**, 239 (1976).

[5] S. Matsumoto, Y. Sato, M. Tsutsumi, and N. Setaka, J. Mater. Sci. **17**, 3106 (1981).

[6] P. K. Bachman, D. Leers, and H. Lydtin, Diamond Relat. Mater. **1**, 1 (1991).

[7] J. C. Angus, H. A. Will, and W. S. Stankop, J. Appl. Phys. **39**, 2915 (1968).

[8] M. Frenklach, J. Appl. Phys. **65**, 5124 (1989).

[9] W. L. Hsu, J. Vac. Sci. Technol. A **6**, 1803 (1988).

[10] Y. Saito, K. Sato, H. Tanaka, K. Fujita, and S. Matsuda, J. Mater. Sci. **23**, 842 (1988).

[11] Y. Liou, A. Inspektor, R. Weimer, D. Knight, and R. Messier, J. Mater. Res. **5**, 2305 (1990).

[12] K. Kobashi, K. Nishimura, K. Miyata, K. Kumagai, and A. Nakaue, J. Mater. Res. **5**, 2469 (1990).

[13] B. R. Stoner, S. R. Sahaida, J. P. Bade, P. Southworth, and P. J. Ellis, J. Mater. Res. **8**, 1334 (1993).

[14] C. Wild, P. Koidl, W. Muller-Sebert, H. Walcher, R. Kohl, N. Herres, R. Locher, R. Samlenski, and R. Brenn, Diamond Relat. Mater. **2**, 158 (1993).

[15] A. van der Drift, Philips Res. Rep. **22**, 267 (1967).

[16] H. Maeda, M. Irie, T. Hino, K. Kusakabe, and S. Morooka, J. Mater. Res. **10**, 158 (1995).

[17] B. Sun, X. Zhang, and Z. Lin, Phys. Rev. B **47**, 9816 (1992).

[18] B. A. Fox, B. R. Stoner, D. M. Maita, P. J. Ellis, R. C. Glass, and F. R. Sivazlian, Diamond Relat. Mater. **3**, 382 (1994).

[19] K. Kobashi, K. Nishimura, K. Miyata, K. Kumagai, and A. Nakaue, J. Mater. Res. **5**, 2469 (1990).

[20] C. Wild, R. Kohl, N. Herres, W. M. Sebert, and P. Koidl, Diamond Relat. Mater. **3**, 373 (1994).

[21] R. Locher, C. Wild, N. Herres, D. Behr, and P. Koidl, Appl. Phys. Lett. **65**, 34 (1994).

[22] S. Jin and T. D. Moustakas, Appl. Phys. Lett. **65**, 403 (1994).

[23] Y. Liou, A. Inspektor, R. Weimer, D. Knight, and R. Messier, J. Mater. Res. **5**, 2305 (1990).

[24] K. Hirabayashi, J. Appl. Phys. **72**, 4083 (1992).

[25] H. C. Shih, C. P. Sung, W. L. Fan, and W. L. Hsu, Thin Solid Films **232**, 41 (1993).

[26] P. Joeris, C. Benndorf, and S. Bohr, J. Appl. Phys. **71**, 4638 (1992).

[27] W. Zhu, A. Inspektor, A. R. Badzian, T. Mckenna, and R. Messier, J. Appl. Phys. **68**, 1489 (1990).

[28] D. M. Gruen, S. Liu, A. R. Krauss, J. Luo, and X. Pan, Appl. Phys. Lett. **64**, 1502 (1994).

[29] D. M. Gruen, X. Pan, A. R. Krauss, A. Liuy, J. Luo, and C. M. Foster, J. Vac. Sci. Technol. A **12**, 1491 (1994).

[30] P. C. Redfern, D. A. Horner, A. A. Curtiss, and D. M. Gruen, J. Phys. Chem. **100**, 11 654 (1996).

[31] D. Zhou, T. G. McCauley, L. C. Qin, A. R. Krauss, and D. M. Gruen, J. Appl. Phys. **83**, 540 (1998).

[32] C. D. Zuiker, A. R. Krauss, D. M. Gruen, X. Pan, J. C. Li, R. Csencsits, A. Erdemir, C. Bindal, and G. Fenske, Thin Solid Films **270**, 154 (1995).

[33] D. Zhou, A. R. Krauss, T. D. Corrigan, T. G. McCauley, R. P. H. Chang, and D. M. Gruen, J. Electrochem. Soc. **144**, L224 (1997).

[34] A. N. Goyette, J. E. Lawler, L. W. Anderson, D. M. Gruen, T. G. McCauley, D. Zhou, and A. R. Krauss, Plasma Sources Sci. Technol. **7**, 149 (1998).

[35] C. D. Zuiker, D. M. Gruen, and A. R. Krauss, J. Appl. Phys. **79**, 3541 (1996).

[36] D. M. Gruen, A. R. Krauss, C. D. Zuiker, R. Csencsits, L. J. Terminello, J. A. Carlisle, I. Jimenez, D. G. J. Sutherland, D. K. Shuh, W. Tong, and F. J. Himpsel, Appl. Phys. Lett. **68**, 1640 (1996).

[37] C. D. Zuiker, A. R. Krauss, D. M. Gruen, J. A. Carlisle, L. J. Terminello, S. A. Asher, and R. W. Bormett, in *Applications of Synchrotron Radiation Techniques to Materials Sciences III*, Proc. of the MRS Symp., edited by L. J. Terminello, S. M. Mini, H. Ade, and D. L. Perry, April 8–12, 1996, San Francisco, CA (MRS, Pittsburgh, PA, 1996), Vol. 432, p. 211.

[38] R. J. Nemanich, J. T. Glass, G. Lucovsky, and R. E. Shroder, J. Vac. Sci. Technol. A **6**, 1783 (1988).

[39] J. Fink, T. M. Heinzerling, J. Pfluger, A. Bubenzer, K. Koidl, and G. Crecelius, Solid State Commun. **47**, 687 (1983).

[40] P. Joeris, I. Schmidt, and C. Benndorf, in *Applications of Diamond Films and Related Materials: Third International Conference*, edited by A. Feldman, Y. Tzeng, W. A. Yarbrough, M. Yoshikawa, M. Murakawa [NIST Spec. Publ. **885**, 381 (1995)].